

Channel Estimation for Beyond Diagonal RIS

Exploiting Core Tensor Sparsity

Daniel C. Araújo, André L. F. de Almeida

Abstract

Beyond diagonal reconfigurable intelligent surface (BD-RIS)s enhance wave manipulation through inter-element couplings but pose significant channel estimation challenges due to cascaded channels and block-Kronecker structures. This work proposes a compressive sensing framework exploiting sparse Tucker decomposition of the measurement tensor and the Kronecker rank-one structure of channel components. Two algorithms are developed: Sparse Tensor Orthogonal Recovery Method (STORM), which uses orthogonal matching pursuit (OMP) for greedy support recovery, and Sparse Tensor subspace-Aided Recovery (STAR), which leverages subspace-based projection for enhanced noise robustness. Both perform joint sparse support identification, followed by a Kronecker rank-one factorization via singular value decomposition (SVD) to recover the channel parameters. Simulations show that STAR achieves oracle-assisted least squares (LS) performance at moderate-to-high signal-to-noise ratio (SNR) with significantly fewer measurements than baseline methods, enabling practical BD-RIS deployment in next-generation millimeter wave (mmWave)/sub-terahertz (sub-THz) networks.

Index Terms

BD-RIS, compressive sensing (CS), mmWave, reconfigurable intelligent surface (RIS)

I. INTRODUCTION

Reconfigurable intelligent surfaces (RISs) have emerged as a transformative technology for sixth-generation (6G) wireless networks, enabling programmable control of electromagnetic wave propagation through planar arrays of low-cost passive elements [1]–[4]. By dynamically adjusting the phase shifts induced by individual surface elements, conventional RISs can perform passive beamforming, enhance coverage, and improve spectral efficiency without requiring active radio-frequency chains [5]–[7]. However, the diagonal scattering matrix structure of conventional RISs, where each element operates independently, fundamentally constrains their wave manipulation flexibility [8].

BD-RISs overcome this limitation by introducing inter-element connections through reconfigurable impedance networks, yielding scattering matrices with non-zero off-diagonal entries [8], [9]. This architectural innovation enables waves absorbed by one element to propagate into neighboring elements, thereby expanding the degrees of freedom for channel engineering [10], [11]. The group-connected architecture organizes elements into groups with tunable intra-group couplings, offering a practical trade-off between performance and hardware complexity [12]. These advances translate into performance improvements, including multi-sector operation for full-space coverage [9] and superior channel gain [11], [13].

Despite these promising advantages, acquiring accurate channel state information (CSI) for BD-RIS-assisted systems is fundamentally more challenging than for conventional RIS due to several factors: (i) the passive nature of RIS elements precludes active pilot processing, necessitating estimation of cascaded transmitter-RIS-receiver channels [14]–[17]; (ii) the inter-element coupling inherent in BD-RIS architectures introduces additional structural constraints that must be leveraged for efficient estimation [18], [19]; and (iii) the large number of RIS elements, particularly in mmWave and sub-THz deployments, leads to prohibitive training overhead if not properly addressed [20].

Recent research has proposed various approaches to tackle these challenges. LS-based methods with optimized pilot sequences minimize estimation error under BD-RIS architectural constraints but require substantial training overhead [18]. Decoupled estimation techniques exploit the block structure of BD-RIS scattering matrices, reducing problem dimensionality at the cost of potential information loss [19]. Semi-blind methods based on PARATUCK tensor decomposition jointly estimate channels and data symbols, avoiding dedicated pilot overhead but with increased algorithmic complexity [21]. More recently, block Tucker decomposition has been applied to BD-RIS channel estimation, yielding performance gains over matrix-based LS methods due to inherent noise rejection [20]. However, existing tensor-based approaches require training overhead proportional to the channel dimensions and do not fully exploit the underlying sparse structure of mmWave/sub-THz channels.

Motivated by the limited scattering nature of high-frequency propagation, CS-based methods have demonstrated significant reductions in training overhead for conventional RIS systems by exploiting channel sparsity in angular domains. For instance, the TRICE framework combines tensor decomposition with ESPRIT-based direction estimation to efficiently recover sparse channels [22]. Other techniques such as OMP leverage common support across users and subcarriers

to recover sparse channel representations with reduced pilot sequences [23], while deep learning-enhanced CS methods further improve recovery accuracy [24]. Nevertheless, direct application of existing CS methods designed for conventional RIS to BD-RIS fails because the block-diagonal scattering structure introduces a unique sparsity pattern in the core tensor that is not captured by standard sparse recovery algorithms.

This paper proposes two novel CS-based algorithms for BD-RIS channel estimation that exploit core tensor sparsity. Both algorithms operate in two stages: first, a sparse support recovery stage identifies active propagation paths using Fourier dictionary matrices; second, a channel parameter estimation stage exploits the Kronecker rank-one structure of each support component through SVD and subspace projection to refine the estimates. Our contributions are:

- We formulate the BD-RIS channel estimation as a sparse core tensor recovery problem and propose two algorithms—STORM and STAR—that combine sparse support recovery with Kronecker rank-one factorization and subspace search, extending CS from conventional RIS to the BD-RIS setting.
- Through extensive simulations, we demonstrate that STAR achieves oracle performance at high SNR while requiring significantly fewer training frames than conventional methods, with computational complexity lower than the TRICE framework [22] adapted to BD-RIS.

II. SYSTEM MODEL

We consider a RIS-assisted system comprising a base station (BS) with N antennas, a RIS with K elements, and a user equipment (UE) with M antennas. The RIS adopts a BD-RIS architecture with Q groups of \bar{K} elements each, where $K = \bar{K}Q$. During training, beam matrices $\mathbf{W}_{\text{tx}} \in \mathbb{C}^{N \times N_{\text{tx}}}$ and $\mathbf{W}_{\text{rx}} \in \mathbb{C}^{M \times M_{\text{rx}}}$ are employed. Let $\mathbf{G} \in \mathbb{C}^{N \times K}$ and $\mathbf{H} \in \mathbb{C}^{M \times K}$ denote the BS-RIS and UE-RIS channels. For the ℓ -th training frame, each group q has scattering matrix $\mathbf{W}_{\text{ris}}^{(q,\ell)} \in \mathbb{C}^{\bar{K} \times \bar{K}}$, forming the block diagonal matrix

$$\mathbf{B}^{(\ell)} = \text{blkdiag} \left[\mathbf{W}_{\text{ris}}^{(1,\ell)}, \dots, \mathbf{W}_{\text{ris}}^{(Q,\ell)} \right]. \quad (1)$$

Defining the processed channels $\bar{\mathbf{H}}_q = \mathbf{W}_{\text{rx}} \mathbf{H}_q \in \mathbb{C}^{M_{\text{rx}} \times \bar{K}}$ and $\bar{\mathbf{G}}_q = \mathbf{W}_{\text{tx}} \mathbf{G}_q \in \mathbb{C}^{N_{\text{tx}} \times \bar{K}}$, the signal during frame ℓ is

$$\mathbf{Y}^{(\ell)} = \sum_{q=1}^Q \bar{\mathbf{H}}_q \mathbf{W}_{\text{ris}}^{(q,\ell)} \bar{\mathbf{G}}_q^T + \mathbf{N}^{(\ell)}, \quad (2)$$

where $\mathbf{N}^{(\ell)}$ is the processed noise matrix. The channels are modeled as $\mathbf{H} = \mathbf{U}_H \mathbf{\Lambda}_H \mathbf{V}_H^H$ and $\mathbf{G} = \mathbf{U}_G \mathbf{\Lambda}_G \mathbf{V}_G^H$, where $\mathbf{U}_H, \mathbf{U}_G$ contain steering vectors at UE and BS, $\mathbf{V}_H, \mathbf{V}_G$ at the RIS, and $\mathbf{\Lambda}_H,$

Λ_G are diagonal path gain matrices with P paths each. We introduce the block Kronecker product operator $\mathbf{A} | \otimes | \mathbf{B} = [\mathbf{A}_1 \otimes \mathbf{B}_1, \dots, \mathbf{A}_Q \otimes \mathbf{B}_Q]$ and define $\bar{\mathbf{V}} = \mathbf{V}_G^H | \otimes | \mathbf{V}_H^H$. By vectorizing (2) and concatenating all K_{ris} training frames, while collecting the vectorized RIS configurations as $\mathbf{w}_{\text{ris}}^{(\ell)} = [\text{vec}(\mathbf{W}_{\text{ris}}^{(1,\ell)})^T, \dots, \text{vec}(\mathbf{W}_{\text{ris}}^{(Q,\ell)})^T]^T$ into $\mathbf{W}_{\text{ris}} = [\mathbf{w}_{\text{ris}}^{(1)}, \dots, \mathbf{w}_{\text{ris}}^{(K_{\text{ris}})}] \in \mathbb{C}^{Q\bar{K}^2 \times K_{\text{ris}}}$, the noise-free received signal across all frames becomes

$$\mathbf{X} = (\mathbf{W}_{\text{tx}} \mathbf{U}_G \otimes \mathbf{W}_{\text{rx}} \mathbf{U}_H) (\Lambda_G \otimes \Lambda_H) \bar{\mathbf{V}} \mathbf{W}_{\text{ris}}, \quad (3)$$

where $\mathbf{X} = [\text{vec}(\mathbf{X}^{(1)}), \dots, \text{vec}(\mathbf{X}^{(K_{\text{ris}})})]$. Taking the transpose reveals a Tucker-3 structure:

$$\mathbf{X}^T = \mathbf{A}_3 \mathbf{D}_{(3)} (\mathbf{A}_2 \otimes \mathbf{A}_1)^T, \quad (4)$$

where $\mathbf{A}_1 = \mathbf{W}_{\text{tx}} \mathbf{U}_G \in \mathbb{C}^{N_{\text{tx}} \times P}$, $\mathbf{A}_2 = \mathbf{W}_{\text{rx}} \mathbf{U}_H \in \mathbb{C}^{M_{\text{rx}} \times P}$, $\mathbf{A}_3 = \mathbf{W}_{\text{ris}}^T \bar{\mathbf{V}}^T \in \mathbb{C}^{K_{\text{ris}} \times P^2}$, and $\mathbf{D}_{(3)} = (\Lambda_G \otimes \Lambda_H)^T$ is the mode-3 unfolding of the core tensor \mathcal{D} . The tensor model is $\mathcal{Y} = \mathcal{X} + \mathcal{N}$, where $\mathcal{Y}, \mathcal{X}, \mathcal{N} \in \mathbb{C}^{N_{\text{tx}} \times M_{\text{rx}} \times K_{\text{ris}}}$.

A conventional LS approach requires $K_{\text{ris}} > Q\bar{K}^2$ frames for identifiability, which becomes prohibitive as \bar{K} grows [20]. However, in mmWave/sub-THz scenarios, $P \ll K$, so \mathcal{D} is sparse and can be recovered with far fewer measurements through CS techniques.

III. PROPOSED CHANNEL ESTIMATION

We propose a CS-based channel estimation algorithm that exploits the sparsity structure of the core tensor \mathcal{D} in (4). The proposed approach consists of two main stages: sparse support recovery and channel parameter estimation.

A. Stage 1: Sparse Support Recovery

We construct discrete Fourier transform (DFT) dictionary matrices $\mathbf{F}_1 \in \mathbb{C}^{N \times N_{\text{grid}}}$, $\mathbf{F}_2 \in \mathbb{C}^{M \times N_{\text{grid}}}$, and $\mathbf{F}_3 = (\mathbf{F}_G^H | \otimes | \mathbf{F}_H^H) \in \mathbb{C}^{Q\bar{K}^2 \times N_{\text{grid}}^2}$ covering all discretized angle bins, where N_{grid} is the grid size. Defining $\bar{\mathbf{A}}_1 = \mathbf{W}_{\text{tx}} \mathbf{F}_1$, $\bar{\mathbf{A}}_2 = \mathbf{W}_{\text{rx}} \mathbf{F}_2$, and $\bar{\mathbf{A}}_3 = \mathbf{W}_{\text{ris}}^T \mathbf{F}_3$, the CS problem is

$$\mathbf{X}_{(3)}^T = \bar{\mathbf{A}}_3 \boldsymbol{\theta} (\bar{\mathbf{A}}_2 \otimes \bar{\mathbf{A}}_1)^T + \mathbf{N}_{(3)}^T, \quad (5)$$

where $\boldsymbol{\theta} \in \mathbb{C}^{N_{\text{grid}}^2 \times N_{\text{tx}} M_{\text{rx}}}$ is the sparse coefficient matrix with only P^2 non-zero rows corresponding to active propagation paths. We propose two strategies:

STORM (OMP-based): Applies OMP to (5) using $\bar{\mathbf{A}}_3$ as dictionary, iteratively selecting atoms with maximum residual correlation over $S = |\mathcal{S}|$ iterations.

STAR (Subspace-based): Computes the SVD of $\mathbf{X}_{(3)}^T$ and identifies the support via the MUSIC-like spectrum

$$\hat{s} = \arg \min_{k \in \{1, \dots, N_{\text{grid}}^2\}} \|\bar{\mathbf{A}}_3(:, k)^H \mathbf{U}_{\text{null}}\|_F^2, \quad (6)$$

selecting the S indices with smallest noise-subspace projection. For both methods, once \mathcal{S} is determined, the coefficients are estimated via $\hat{\boldsymbol{\theta}}_{\mathcal{S}} = \bar{\mathbf{A}}_{3, \mathcal{S}}^\dagger \mathbf{X}_{(3)}^T$.

B. Stage 2: Channel Parameter Estimation

For each support index $s \in \mathcal{S}$, we extract the coefficient vector $\mathbf{d}_s = (\mathbf{A}_2 \otimes \mathbf{A}_1)^T \hat{\boldsymbol{\theta}}_{:,s}$ and reshape it into $\mathbf{M}_s \in \mathbb{C}^{N_{\text{tx}} \times M_{\text{rx}}}$. Since each column of $\mathbf{D}_{(3)} = (\boldsymbol{\Lambda}_G \otimes \boldsymbol{\Lambda}_H)^T$ corresponds to a single path pair (p_G, p_H) , \mathbf{M}_s exhibits a rank-one structure:

$$\mathbf{M}_s = \mathbf{A}_1(:, p_G) \mathbf{A}_2(:, p_H)^T. \quad (7)$$

Performing SVD on $\mathbf{M}_s = \mathbf{U}_s \boldsymbol{\Sigma}_s \mathbf{V}_s^H$ and defining noise subspaces \mathbf{U}_{null} and \mathbf{V}_{null} from the trailing $(N_{\text{tx}} - 1)$ and $(M_{\text{rx}} - 1)$ singular vectors of \mathbf{U}_s and \mathbf{V}_s , respectively, we estimate the path indices via

$$\begin{aligned} \hat{p}_{\text{tx}} &= \arg \min_{i \in \{1, \dots, N_{\text{grid}}\}} \|\bar{\mathbf{A}}_1(:, i)^H \mathbf{V}_{\text{null}}\|_F^2, \\ \hat{p}_{\text{rx}} &= \arg \min_{j \in \{1, \dots, N_{\text{grid}}\}} \|\bar{\mathbf{A}}_2(:, j)^H \mathbf{U}_{\text{null}}\|_F^2, \end{aligned} \quad (8)$$

and compute the core tensor entry as $\hat{d}_s = \bar{\mathbf{A}}_1(:, \hat{p}_{\text{tx}})^H \mathbf{M}_s \bar{\mathbf{A}}_2(:, \hat{p}_{\text{rx}})^*$. After processing all $s \in \mathcal{S}$, the entries \hat{d}_s form $\hat{\mathbf{D}}_{(3), \mathcal{S}} = \text{diag}(\hat{d}_1, \dots, \hat{d}_{|\mathcal{S}|})$, and the estimated composite channel is

$$\widehat{\mathbf{G}} \otimes \widehat{\mathbf{H}} = \mathbf{F}_{3, \mathcal{S}} \hat{\mathbf{D}}_{(3), \mathcal{S}} (\mathbf{F}_{2, \mathcal{S}} \otimes \mathbf{F}_{1, \mathcal{S}})^T. \quad (9)$$

Algorithms 1 and 2 summarize the complete procedures for STORM and STAR, highlighting the Stage 1 difference that governs the performance trade-off between the two methods.

C. Computational Complexity Analysis

We analyze the computational complexity of the proposed STORM and STAR algorithms in terms of floating-point operations. Let $S = |\mathcal{S}|$ denote the cardinality of the estimated support set, N_{grid} represent the size of the discretized angle grid, and P denote the number of true propagation paths per channel.

Algorithm 1 STORM: OMP-based sparse tensor recovery

Require: $\mathbf{X}_{(3)}^T$, dictionaries $\bar{\mathbf{A}}_1, \bar{\mathbf{A}}_2, \bar{\mathbf{A}}_3$, sparsity S
Ensure: Estimated composite channel $\widehat{\mathbf{G}} \otimes \widehat{\mathbf{H}}$
Stage 1: OMP-based support recovery

- 1: $\mathcal{S} \leftarrow \emptyset, \mathbf{R} \leftarrow \mathbf{X}_{(3)}^T$
- 2: **for** $t = 1, \dots, S$ **do**
- 3: $k^* \leftarrow \arg \max_k \|\bar{\mathbf{A}}_3(:, k)^H \mathbf{R}\|_F$ ▷ correlation
- 4: $\mathcal{S} \leftarrow \mathcal{S} \cup \{k^*\}$
- 5: $\hat{\boldsymbol{\theta}}_{\mathcal{S}} \leftarrow \bar{\mathbf{A}}_{3, \mathcal{S}}^\dagger \mathbf{X}_{(3)}^T$ ▷ LS update
- 6: $\mathbf{R} \leftarrow \mathbf{X}_{(3)}^T - \bar{\mathbf{A}}_{3, \mathcal{S}} \hat{\boldsymbol{\theta}}_{\mathcal{S}}$ ▷ residual update
- 7: **end for**

Stage 2: Kronecker rank-one factorization

- 8: **for each** $s \in \mathcal{S}$ **do**
 - 9: Reshape $\hat{\boldsymbol{\theta}}_{\mathcal{S}(s),:}^T$ into $\mathbf{M}_s \in \mathbb{C}^{N_{\text{tx}} \times M_{\text{rx}}}$
 - 10: $[\mathbf{U}_s, \boldsymbol{\Sigma}_s, \mathbf{V}_s] \leftarrow \text{SVD}(\mathbf{M}_s)$
 - 11: $\mathbf{U}_{\text{null}}^{(s)} \leftarrow$ trailing $(N_{\text{tx}} - 1)$ cols. of \mathbf{U}_s
 - 12: $\mathbf{V}_{\text{null}}^{(s)} \leftarrow$ trailing $(M_{\text{rx}} - 1)$ cols. of \mathbf{V}_s
 - 13: Estimate $\hat{p}_{\text{tx}}, \hat{p}_{\text{rx}}$ via (8)
 - 14: $\hat{d}_s \leftarrow \bar{\mathbf{A}}_1(:, \hat{p}_{\text{tx}})^H \mathbf{M}_s \bar{\mathbf{A}}_2(:, \hat{p}_{\text{rx}})^*$
 - 15: **end for**
 - 16: $\hat{\mathbf{D}}_{(3), \mathcal{S}} \leftarrow \text{diag}(\hat{d}_1, \dots, \hat{d}_{|\mathcal{S}|})$
 - 17: **return** $\mathbf{F}_{3, \mathcal{S}} \hat{\mathbf{D}}_{(3), \mathcal{S}} (\mathbf{F}_{2, \mathcal{S}} \otimes \mathbf{F}_{1, \mathcal{S}})^T$
-

The OMP-based support recovery in STORM requires computing correlations between the residual and all dictionary atoms at each iteration. For each of the S iterations, the algorithm performs matrix-vector multiplications involving $\bar{\mathbf{A}}_3 \in \mathbb{C}^{K_{\text{ris}} \times N_{\text{grid}}^2}$ and $(\bar{\mathbf{A}}_2 \otimes \bar{\mathbf{A}}_1)^T \in \mathbb{C}^{N_{\text{grid}} \times N_{\text{tx}} M_{\text{rx}}}$, followed by a least squares update. The dominant cost per iteration is $\mathcal{O}(K_{\text{ris}} N_{\text{grid}}^2 N_{\text{tx}} M_{\text{rx}})$, yielding a total Stage 1 complexity of

$$C_{\text{Stage 1}}^{\text{STORM}} = \mathcal{O}(SK_{\text{ris}} N_{\text{grid}}^2 N_{\text{tx}} M_{\text{rx}}). \quad (10)$$

For STAR, which employs a subspace-based approach instead of greedy selection, the Stage 1 complexity remains comparable, since both methods must identify the sparse support from the

Algorithm 2 STAR: Subspace-based sparse tensor recovery

Require: $\mathbf{X}_{(3)}^T$, dictionaries $\bar{\mathbf{A}}_1, \bar{\mathbf{A}}_2, \bar{\mathbf{A}}_3$, sparsity S
Ensure: Estimated composite channel $\widehat{\mathbf{G}} \otimes \widehat{\mathbf{H}}$
Stage 1: Subspace-based support recovery

- 1: $[\mathbf{U}, \boldsymbol{\Sigma}, \mathbf{V}] \leftarrow \text{SVD}(\mathbf{X}_{(3)}^T)$
- 2: $\mathbf{U}_{\text{null}} \leftarrow$ trailing $(K_{\text{ris}} - S)$ columns of \mathbf{U}
- 3: **for** $k = 1, \dots, N_{\text{grid}}^2$ **do**
- 4: $f(k) \leftarrow \|\bar{\mathbf{A}}_3(:, k)^H \mathbf{U}_{\text{null}}\|_F^2$ ▷ MUSIC spectrum
- 5: **end for**
- 6: $\mathcal{S} \leftarrow$ indices of the S smallest $f(k)$
- 7: $\hat{\boldsymbol{\theta}}_{\mathcal{S}} \leftarrow \bar{\mathbf{A}}_{3,\mathcal{S}}^\dagger \mathbf{X}_{(3)}^T$

Stage 2: Execute Stage 2 of Algorithm 1 (Steps 8–14)

same dictionary structure.

Stage 2 is identical for both STORM and STAR. For each of the S identified support indices, Stage 2 performs the following operations: (i) computing the pseudoinverse $\bar{\mathbf{A}}_{3,\mathcal{S}}^\dagger$, which has complexity $\mathcal{O}(\min(K_{\text{ris}}, S)^2 \max(K_{\text{ris}}, S))$ when computed once for the entire support set; (ii) reshaping and SVD of $\mathbf{M}_s \in \mathbb{C}^{N_{\text{tx}} \times M_{\text{rx}}}$, with complexity $\mathcal{O}(N_{\text{tx}} M_{\text{rx}} \min(N_{\text{tx}}, M_{\text{rx}}))$ per support index; and (iii) noise subspace search over the dictionary atoms as in (8), which projects all columns of $\bar{\mathbf{A}}_1$ and $\bar{\mathbf{A}}_2$ onto the noise subspaces $\mathbf{V}_{\text{null}} \in \mathbb{C}^{N_{\text{tx}} \times (N_{\text{tx}} - 1)}$ and $\mathbf{U}_{\text{null}} \in \mathbb{C}^{M_{\text{rx}} \times (M_{\text{rx}} - 1)}$, requiring $\mathcal{O}(N_{\text{grid}}(N_{\text{tx}}^2 + M_{\text{rx}}^2))$ operations per index. Aggregating over all S support indices, the total Stage 2 complexity is $\mathcal{O}(SN_{\text{grid}}(N_{\text{tx}}^2 + M_{\text{rx}}^2))$.

Since $S \ll N_{\text{grid}}^2$ due to channel sparsity, and assuming $K_{\text{ris}} \ll Q\bar{K}^2$ for compressive measurements, the total complexity is dominated by Stage 1 when N_{grid} is large. Compared to the TRICE framework [22], which requires tensor decomposition operations with complexity $\mathcal{O}(K_{\text{ris}}^2 Q \bar{K}^2 N_{\text{tx}} M_{\text{rx}})$ for full tensor factorization, the proposed methods achieve lower complexity by exploiting the Kronecker rank-one structure and avoiding explicit full-rank tensor decomposition. The key difference between STORM and STAR lies exclusively in the Stage 1 support recovery strategy: STORM employs greedy OMP, which iteratively selects atoms based on correlation with the residual, achieving fast convergence in high-SNR regimes, whereas STAR uses a subspace-based method that identifies the support via noise subspace orthogonality

TABLE I
COMPUTATIONAL COMPLEXITY COMPARISON

Method	Stage 1	Stage 2
STORM	$\mathcal{O}(SK_{\text{ris}}N_{\text{grid}}^2N_{\text{tx}}M_{\text{rx}})$	$\mathcal{O}(SN_{\text{grid}}(N_{\text{tx}}^2 + M_{\text{rx}}^2))$
STAR	$\mathcal{O}(SK_{\text{ris}}N_{\text{grid}}^2N_{\text{tx}}M_{\text{rx}})$	$\mathcal{O}(SN_{\text{grid}}(N_{\text{tx}}^2 + M_{\text{rx}}^2))$
Vectorized CS	$\mathcal{O}(SK_{\text{ris}}N_{\text{tx}}M_{\text{rx}}N_{\text{grid}}^4)$	—
TRICE [22]	$\mathcal{O}(K_{\text{ris}}^2Q\bar{K}^2N_{\text{tx}}M_{\text{rx}})$	$\mathcal{O}(K_{\text{ris}}Q\bar{K}^2)$

(MUSIC-like), providing superior robustness to noise, especially in low-SNR conditions. Once the support is identified, both methods proceed identically through Stage 2, as reflected in the simulation results presented in the next section.

Table I summarizes the computational complexity comparison among different methods. As matter of comparison, we analyze the vectorized CS approach, which applies OMP directly to the flattened tensor measurement vector of dimension $K_{\text{ris}}N_{\text{tx}}M_{\text{rx}}$, constructing a dictionary via the Khatri-Rao product $\text{KR}(\mathbf{A}_1 \otimes \mathbf{A}_2, \mathbf{A}_3)$ with N_{grid}^4 atoms, covering all possible angle combinations across the three tensor modes. This single-stage OMP approach incurs prohibitively high complexity $\mathcal{O}(SK_{\text{ris}}N_{\text{tx}}M_{\text{rx}}N_{\text{grid}}^4)$ that scales quartically with the grid size and does not benefit from the two-stage decomposition. In contrast, by exploiting the tensor structure and Kronecker factorization, STORM and STAR reduce the dictionary size from N_{grid}^4 to N_{grid}^2 , achieving a quadratic reduction in complexity. The TRICE framework, while also exploiting tensor structure, incurs a higher Stage 1 cost because it performs full tensor decomposition without exploiting core tensor sparsity. As shown in the table, STORM and STAR share identical Stage 2 complexity.

IV. NUMERICAL RESULTS

We evaluate the proposed channel estimation scheme through Monte Carlo simulations. We report the normalized mean squared error (NMSE) as a function of the SNR, the NMSE as a function of the percentage of RIS measurements relative to $Q\bar{K}^2$, and the processing time of the algorithms as a function of \bar{K} . Expressing the measurement size as a percentage of $Q\bar{K}^2$ allows a fair comparison across different BD-RIS configurations: by fixing the ratio between the number of measurements and the total number of unknown coefficients $Q\bar{K}^2$, we keep the proportion between sparsity and measurement budget equivalent when varying \bar{K} and Q . The

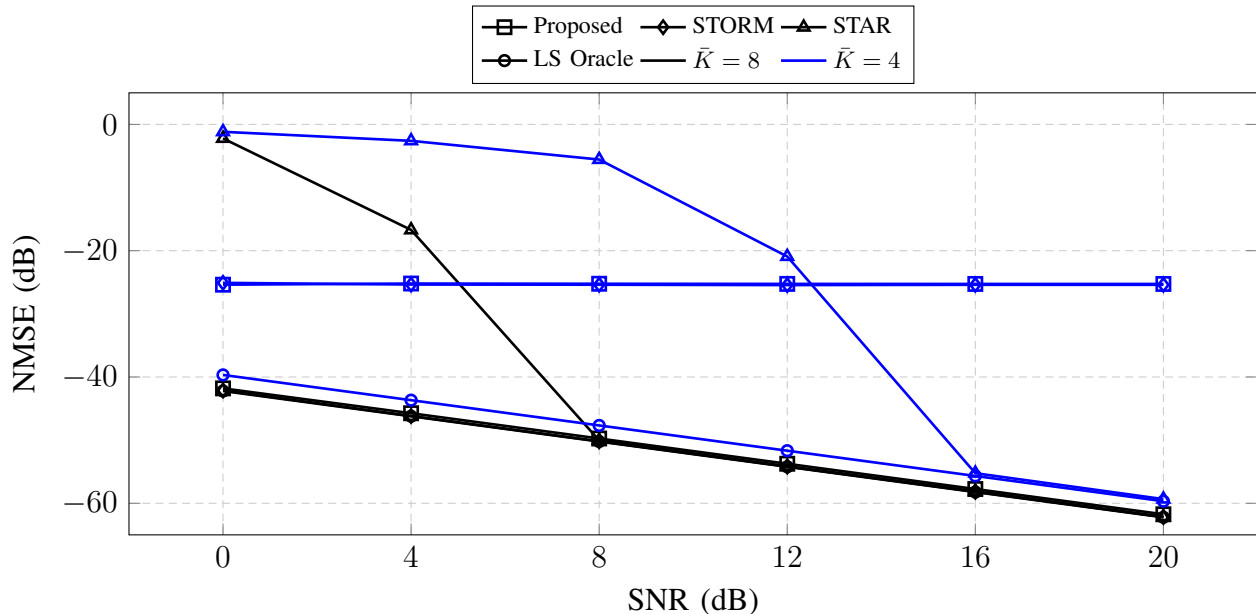


Fig. 1. NMSE as a function of SNR. Fixed: $N = 32$, $M = 32$, $K = 64$, $N_{\text{tx}} = 16$, $M_{\text{rx}} = 16$; RIS measurement size at 50% of $Q\bar{K}^2$.

simulation setup is as follows. The BS and UE are equipped with $N = 32$ and $M = 32$ antennas, respectively, and the RIS has $K = 64$ elements. The number of training beams at the transmitter and receiver is $N_{\text{tx}} = 16$ and $M_{\text{rx}} = 16$. We consider $\bar{K} \in \{4, 8\}$ elements per group, and the number of propagation paths is set accordingly to reflect a sparse channel. The number of RIS training frames K_{ris} is chosen as a fraction of $Q\bar{K}^2$ when evaluating NMSE versus the percentage of measurements. We compare the following algorithms: the proposed STORM and STAR methods, the TRICE framework [22] adapted to BD-RIS, and LS Oracle (LSO), which assumes perfect knowledge of the support and serves as a lower bound.

Fig. 1 shows the NMSE versus SNR. The curves reflect the impact of \bar{K} : a larger \bar{K} offers greater robustness at low SNR, with a smaller NMSE gap to the bound in that regime compared with $\bar{K} = 4$. For $\bar{K} = 8$, all algorithms converge to the LSO bound as the SNR increases, confirming that the measurement budget at 50% compression is sufficient for accurate sparse recovery when the group size provides enough diversity. For $\bar{K} = 4$, only the subspace-based method STAR attains the bound at high SNR, whereas the greedy-search-based algorithms, such as TRICE [22] and STORM, saturate and do not reach oracle performance. This saturation is

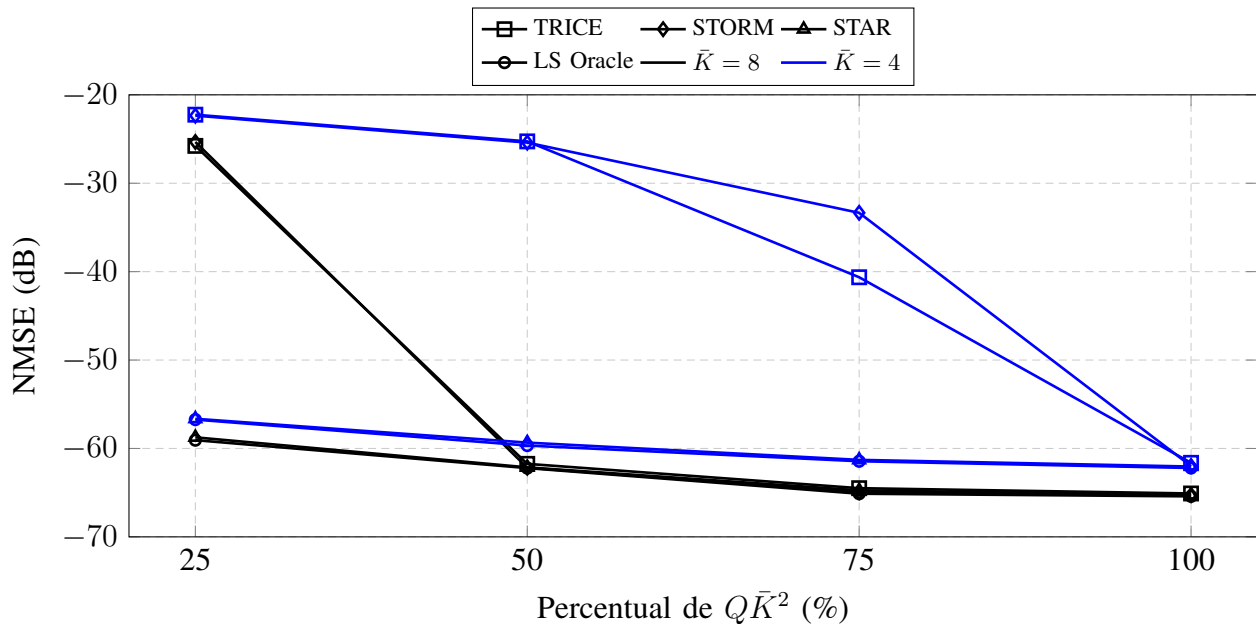


Fig. 2. NMSE as a function of the percentage of RIS measurements relative to $Q\bar{K}^2$. Fixed: $N = 32$, $M = 32$, $K = 64$, $N_{\text{tx}} = 16$, $M_{\text{rx}} = 16$.

attributed to reduced dictionary coherence in smaller groups, which degrades the accuracy of atom selection in OMP-based methods.

Fig. 2 plots the NMSE versus the fraction of $Q\bar{K}^2$ used as measurements. The LSO bound improves as the percentage increases due to the larger effective aperture of the measurement matrix. For $\bar{K} = 8$, all algorithms converge to the bound as the measurement fraction grows, indicating that even moderate compression ratios (30–50%) are sufficient for reliable sparse recovery. Notably, STAR achieves near-oracle performance across both group sizes: for $\bar{K} = 4$, STAR tracks the LSO bound closely even under heavy compression, whereas STORM exhibits a larger gap. This demonstrates that the subspace-based approach of STAR provides superior robustness to the reduced degrees of freedom in smaller group configurations compared to the greedy OMP-based strategy of STORM. From a practical standpoint, these results suggest that BD-RIS systems can operate with significantly fewer training frames than the $Q\bar{K}^2$ required by conventional LS methods, freeing resources for data transmission.

Fig. 3 reports the processing time versus \bar{K} . The proposed Kronecker rank-one methods STORM and STAR remain computationally cheaper than TRICE across the range of \bar{K} , with a

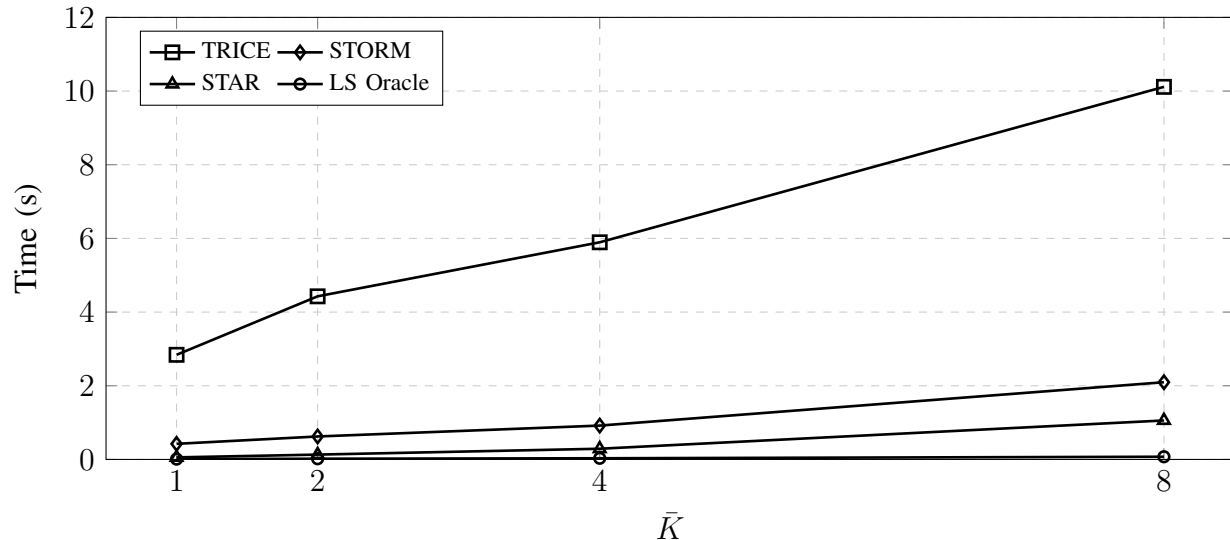


Fig. 3. Processing time of the algorithms as a function of \bar{K} . Fixed: $N = 32$, $M = 32$, $K = 64$, $N_{\text{tx}} = 16$, $M_{\text{rx}} = 16$; RIS measurement size at 50% of $Q\bar{K}^2$.

slight advantage for the subspace-based method STAR, which exhibits the lowest runtime among all algorithms.

Fig. 4 shows the NMSE versus the number of paths per channel with a fixed number of measurements at 50% of $Q\bar{K}^2$. As P increases, all algorithms experience performance degradation because the effective sparsity level decreases; the measurement budget remains constant while the number of unknowns grows as P^2 . This imbalance is particularly evident for STAR, which exhibits a steeper degradation curve than STORM. This behavior arises because the subspace-based support identification in STAR relies on clear separation between the signal and noise subspaces, which deteriorates when the core tensor is less sparse. Nevertheless, for the typical path counts encountered in mmWave and sub-THz environments ($P \leq 4$), both proposed methods maintain NMSE well below -20 dB, confirming their suitability for practical deployment scenarios.

V. CONCLUSION

This paper addressed the channel estimation problem for BD-RIS-assisted wireless systems by formulating it as a sparse core tensor recovery problem that exploits the limited-scattering properties of mmWave and sub-THz channels. We proposed two novel algorithms, STORM and STAR, that leverage Kronecker rank-one factorization to estimate sparse channels with reduced

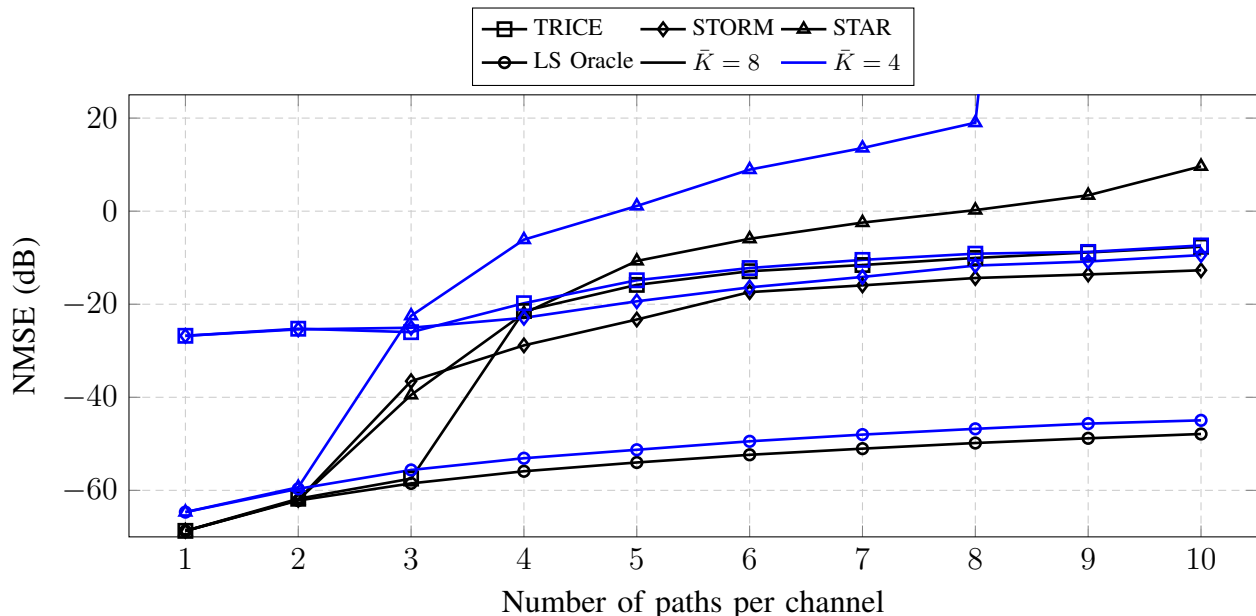


Fig. 4. NMSE as a function of the number of paths per channel. Fixed: $N = 32$, $M = 32$, $K = 64$, $N_{\text{tx}} = 16$, $M_{\text{rx}} = 16$; RIS measurement size at 50% of $Q\bar{K}^2$.

training overhead compared to existing methods. Simulations demonstrated that both algorithms achieve near-oracle NMSE performance, with STAR attaining the oracle bound at high SNR even for smaller group sizes while maintaining lower computational complexity than the TRICE framework adapted to BD-RIS. The results revealed that a minimum group size \bar{K} is necessary to fully exploit channel sparsity, with systems operating at $\bar{K} = 8$ achieving substantial compression gains without sacrificing estimation accuracy. Future work includes extending the framework to wideband OFDM systems with frequency-selective channels, and exploring hybrid architectures that combine group-connected and fully-connected BD-RIS topologies.

REFERENCES

- [1] S. Gong, X. Lu, D. T. Hoang, D. Niyato, L. Shu, D. I. Kim, and Y.-C. Liang, "Toward smart wireless communications via intelligent reflecting surfaces: A contemporary survey," *IEEE Communications Surveys & Tutorials*, vol. 22, no. 4, pp. 2283–2314, 2020.
- [2] Q. Wu, S. Zhang, B. Zheng, C. You, and R. Zhang, "Intelligent reflecting surface-aided wireless communications: A tutorial," *IEEE Transactions on Communications*, vol. 69, no. 5, pp. 3313–3351, 2021.
- [3] Y. Liu, X. Liu, X. Mu, T. Hou, J. Xu, M. Di Renzo, and N. Al-Dhahir, "Reconfigurable intelligent surfaces: Principles and opportunities," *IEEE Communications Surveys & Tutorials*, vol. 23, no. 3, pp. 1546–1577, 2021.
- [4] H. Li, M. Nerini, S. Shen, and B. Clerckx, "A tutorial on beyond-diagonal reconfigurable intelligent surfaces: Modeling, architectures, system design and optimization, and applications," *IEEE Communications Surveys & Tutorials*, vol. 28, pp. 4086–4126, 2026.
- [5] C. Huang, A. Zappone, G. C. Alexandropoulos, M. Debbah, and C. Yuen, "Reconfigurable intelligent surfaces for energy efficiency in wireless communication," *IEEE Transactions on Wireless Communications*, vol. 18, no. 8, pp. 4157–4170, 2019.

- [6] Q. Wu and R. Zhang, "Beamforming optimization for wireless network aided by intelligent reflecting surface with discrete phase shifts," *IEEE Transactions on Communications*, vol. 68, no. 3, pp. 1838–1851, 2020.
- [7] Q. Tao, Z. Li, K. Zhi, S. Li, W. Yuan, L. Zaniboni, S. Stanczak, E. Viterbo, and X. Wang, "A survey on reconfigurable intelligent surface-assisted orthogonal time frequency space systems," *IEEE Open Journal of Vehicular Technology*, vol. 6, pp. 1881–1909, 2025.
- [8] H. Li, S. Shen, M. Nerini, and B. Clerckx, "Reconfigurable intelligent surfaces 2.0: Beyond diagonal phase shift matrices," *IEEE Communications Magazine*, vol. 62, no. 3, pp. 102–108, 2024.
- [9] H. Li, S. Shen, and B. Clerckx, "Beyond diagonal reconfigurable intelligent surfaces: A multi-sector mode enabling highly directional full-space wireless coverage," *IEEE Journal on Selected Areas in Communications*, vol. 41, no. 8, pp. 2446–2460, 2023.
- [10] M. Nerini, S. Shen, H. Li, and B. Clerckx, "Beyond diagonal reconfigurable intelligent surfaces utilizing graph theory: Modeling, architecture design, and optimization," *IEEE Transactions on Wireless Communications*, vol. 23, no. 8, pp. 9972–9985, 2024.
- [11] H. Li, S. Shen, M. Nerini, M. Di Renzo, and B. Clerckx, "Beyond diagonal reconfigurable intelligent surfaces with mutual coupling: Modeling and optimization," *IEEE Communications Letters*, vol. 28, no. 4, pp. 937–941, 2024.
- [12] P. Del Hougne, "Physics-compliant diagonal representation of beyond-diagonal ris," in *2024 IEEE 25th International Workshop on Signal Processing Advances in Wireless Communications (SPAWC)*, 2024, pp. 931–935.
- [13] Y. Peng, H. Li, Z. Wu, and B. Clerckx, "Lossy beyond diagonal reconfigurable intelligent surfaces: Modeling and optimization," *IEEE Transactions on Wireless Communications*, vol. 25, pp. 7365–7380, 2026.
- [14] B. Zheng, C. You, W. Mei, and R. Zhang, "A survey on channel estimation and practical passive beamforming design for intelligent reflecting surface aided wireless communications," *IEEE Communications Surveys & Tutorials*, vol. 24, no. 2, pp. 1035–1071, 2022.
- [15] A. L. Swindlehurst, G. Zhou, R. Liu, C. Pan, and M. Li, "Channel estimation with reconfigurable intelligent surfaces—a general framework," *Proceedings of the IEEE*, vol. 110, no. 9, pp. 1312–1338, 2022.
- [16] G. T. de Araújo and A. L. F. de Almeida, "PARAFAC-based channel estimation for intelligent reflective surface assisted mimo system," in *2020 IEEE 11th Sensor Array and Multichannel Signal Processing Workshop (SAM)*, 2020, pp. 1–5.
- [17] G. T. de Araújo, A. L. F. de Almeida, and R. Boyer, "Channel estimation for intelligent reflecting surface assisted mimo systems: A tensor modeling approach," *IEEE Journal of Selected Topics in Signal Processing*, vol. 15, no. 3, pp. 789–802, 2021.
- [18] H. Li, S. Shen, Y. Zhang, and B. Clerckx, "Channel estimation and beamforming for beyond diagonal reconfigurable intelligent surfaces," *IEEE Transactions on Signal Processing*, vol. 72, pp. 3318–3332, 2024.
- [19] B. Sokal, Fazal-E-Asim, A. L. F. de Almeida, H. Li, and B. Clerckx, "A decoupled channel estimation method for beyond diagonal ris," in *2024 58th Asilomar Conference on Signals, Systems, and Computers*, 2024, pp. 1395–1399.
- [20] A. L. F. de Almeida, B. Sokal, H. Li, and B. Clerckx, "Channel estimation for beyond diagonal ris via tensor decomposition," *IEEE Transactions on Signal Processing*, vol. 73, pp. 4764–4779, 2025.
- [21] G. T. de Araújo and A. L. F. de Almeida, "Semi-blind channel estimation for beyond diagonal ris," in *2024 58th Asilomar Conference on Signals, Systems, and Computers*, 2024, pp. 1586–1590.
- [22] K. Ardah, S. Gherekhloo, A. L. F. de Almeida, and M. Haardt, "TRICE: A Channel Estimation Framework for RIS-Aided Millimeter-Wave MIMO Systems," *IEEE Signal Processing Letters*, vol. 28, pp. 513–517, 2021.
- [23] A. Abdallah, A. Celik, M. M. Mansour, and A. M. Eltawil, "RIS-aided mmWave MIMO channel estimation using deep learning and compressive sensing," *IEEE Transactions on Wireless Communications*, vol. 22, no. 5, pp. 3503–3521, 2023.
- [24] P. M. Soumya, R. Ganiga, S. Hiremath, and M. B. Teklu, "Integration of deep learning and compressive sensing algorithm for beamspace channel estimation in mmWave massive MIMO systems," *IEEE Access*, vol. 13, pp. 181 200–181 216, 2025.